






$\Lambda\Lambda$ pairing effects in spherical and deformed multi- Λ hyperisotopesJing Guo (郭静) ¹, C. F. Chen (陈超锋) ¹, Xian-Rong Zhou (周先荣) ^{1,*}, Q. B. Chen (陈启博) ¹ and H.-J. Schulze ²¹*Department of Physics, East China Normal University, Shanghai 200241, China*²*INFN Sezione di Catania, Dipartimento di Fisica, Università di Catania, Via Santa Sofia 64, 95123 Catania, Italy*

(Received 17 December 2021; accepted 4 March 2022; published 22 March 2022)

The $\Lambda\Lambda$ pairing effects in spherical and deformed multi- Λ hyperisotopes are investigated in the framework of the Skyrme-Hartree-Fock approach employing a δ pairing force with the pairing strength of Λ hyperons being 4/9 of that for nucleons. For spherical hyperisotopes, the occurrences of magic numbers $-S = 2, 8, 18, 20, 34, 58, 68,$ and 70 , which are attributed to a Woods-Saxon-like Λ hyperon potential, are evinced by the sudden drop of 2Λ separation energies and the vanishing pairing gaps and pairing energies. The results are compared with equivalent ones in recent Hartree-Fock-Bogoliubov and relativistic-Hartree-Bogoliubov calculations. For the deformed hyperisotopes, more possible Λ hyperon magic numbers $-S = 4, 6, 10, 14, 26, 30,$ and 32 are found based on the analysis of the single-particle energy levels, and are all sensitive to the quadrupole deformation β_2 . The steps of the 2Λ separation energies are accordingly smaller than in spherical hyperisotopes, and the possibilities for pairing are consistently reduced.

DOI: [10.1103/PhysRevC.105.034322](https://doi.org/10.1103/PhysRevC.105.034322)**I. INTRODUCTION**

Since the first hypernucleus was discovered in a stack of photographic emulsions exposed to cosmic rays by Danysz and Pniewski in 1953 [1], the study of hypernuclei has become an important topic in nuclear physics. Most of the produced hypernuclei are single- Λ hypernuclei, and also a few light double- Λ hypernuclei are known [2–5]. Due to the limited amount of data, the interactions between hyperons still remain an open question.

In the past few decades, many theoretical studies of hypernuclei have been performed adopting various approaches, such as nonrelativistic Skyrme-Hartree-Fock (SHF) [6–15], relativistic mean-field (RMF) [16–27], Hartree-Fock-Bogoliubov (HFB) [28], Brueckner-Hartree-Fock (BHF) [29–32], beyond-mean-field approach [33–39], cluster model [40,41], and the Jacobi no-core shell approach [42]. Most of them predicted the binding energies and Λ separation energies in fair agreement with the experimental data for the single- Λ systems. To make predictions for the multi- Λ hypernuclei, reliable ΛN and $\Lambda\Lambda$ interactions are necessary, which were studied in Refs. [5,18,27,30,31,37,43], for example.

Moreover, the pairing interactions between Λ hyperons can play an important role in hypothetical multi- Λ hypernuclei. As there are currently no direct experimental data on this phenomenon, and also reliable theoretical calculations of the Λ pairing gap are not possible due to lack of information (phase shifts) on the bare $\Lambda\Lambda$ interaction, these studies can only be speculative for the time being, making reasonable assumptions for the relevant input quantities, and no precise quantitative predictions can be expected. In this sense, the

$\Lambda\Lambda$ pairing effects in hypernuclear matter have been explored within the BCS approximation for some time [44–48], with so far inconclusive results [48], even regarding the mere existence of pairing.

Nevertheless, recently even the more complex problem of $\Lambda\Lambda$ pairing in finite hypernuclei has been addressed theoretically. In Ref. [28] the $\Lambda\Lambda$ pairing in multi- Λ hyperisotopes of Ca, Sn, and Pb was investigated within a HFB model. The strength of $\Lambda\Lambda$ pairing was calibrated to match the maximal value of the prediction of the $\Lambda\Lambda$ pairing gap in uniform matter for densities and isospin asymmetries equivalent to those existing in multi- Λ hypernuclei [49], so that upper bounds for the prediction of the Λ pairing gap and its effects in hypernuclei were provided.

The same multi- Λ hyperisotopes of Ca, Sn, and Pb were then studied in a relativistic-Hartree-Bogoliubov (RHB) calculation [50], where a relation between the effective pairing interactions for Λ hyperons and for nucleons based on the quark model was proposed instead, namely, the strength of the Λ pairing interaction being 4/9 of that for nucleons. It was found that the $\Lambda\Lambda$ pairing gaps of the three hypernuclei $^{46}_{6\Lambda}\text{Ca}$, $^{160}_{28\Lambda}\text{Sn}$, and $^{272}_{64\Lambda}\text{Pb}$ are smaller and decrease faster with mass number A than those in HFB [28]. Whether these differences originate only from the different $\Lambda\Lambda$ pairing strengths or also from the different ΛN interactions and theoretical methods remains an open question. Moreover, only spherical hypernuclei were treated in Refs. [28,50]. The role of $\Lambda\Lambda$ pairing effects in deformed hypernuclei is thus an interesting problem that we will study here.

The purpose of the present work is twofold. First, we extend the method of determining the $\Lambda\Lambda$ pairing strength proposed in the RHB model [50] to the nonrelativistic SHF model and apply it to the multi- Λ Ca, Sn, and Pb hypernuclei to compare with the results obtained by HFB [28] and RHB

*xrzhou@phy.ecnu.edu.cn

[50]. Next, we use that pairing force and study the pairing effects in multi- Λ isotopes of the typical deformed-core nuclei ^{24}Mg , ^{56}Fe , and ^{104}Zr [51–54] in detail. For the mean-field part, we use the same parameters as HFB [28], i.e., Skyrme force SLy5 for the NN part [55] and Nijmegen interactions NSC89, NSC97a, and NSC97f for the ΛN part [30,31], and the empirical prescription EmpC for the $\Lambda\Lambda$ interaction [56]. The strength of the residual $\Lambda\Lambda$ pairing interaction is set to 4/9 of that for nucleons, as in Ref. [50].

II. FORMALISM

The main purpose of the present work is to investigate $\Lambda\Lambda$ pairing effects in spherical and deformed multi- Λ hypernuclei in the SHF framework. In this approach, the total energy of a hypernucleus is given by an energy density functional [6,8,29,31],

$$E = \int d^3r \varepsilon(\mathbf{r}), \quad \varepsilon = \varepsilon_{NN} + \varepsilon_{\Lambda N} + \varepsilon_{\Lambda\Lambda}, \quad (1)$$

where ε_{NN} , $\varepsilon_{\Lambda N}$, and $\varepsilon_{\Lambda\Lambda}$ account for the nucleon-nucleon, hyperon-nucleon, and hyperon-hyperon interactions, respectively. The functional depends on the one-body densities ρ_q , kinetic densities τ_q , and spin-orbit currents \mathbf{J}_q ,

$$[\rho_q, \tau_q, \mathbf{J}_q] = \sum_{k=1}^{N_q} n_q^k [|\phi_q^k|^2, |\nabla\phi_q^k|^2, \phi_q^{k*}(\nabla\phi_q^k \times \boldsymbol{\sigma})/i], \quad (2)$$

where ϕ_q^k ($k = 1, \dots, N_q$) are the self-consistently calculated single-particle (s.p.) wave functions of the N_q occupied states for the species $q = n, p, \Lambda$ in a hypernucleus. They satisfy the Schrödinger equation, obtained by the minimization of the total energy functional (1) according to the variational principle,

$$\left[\nabla \cdot \frac{1}{2m_q^*} \nabla - V_q(\mathbf{r}) + i\mathbf{W}_q(\mathbf{r}) \cdot (\nabla \times \boldsymbol{\sigma}) \right] \phi_q^k(\mathbf{r}) = e_q^k \phi_q^k(\mathbf{r}), \quad (3)$$

in which $\mathbf{W}_q(\mathbf{r})$ is the spin-orbit interaction part for the nucleons as given in Refs. [57,58], while the spin-orbit force for the Λ hyperon is very small [15,59,60] and not included in the present study. The central mean fields $V_q(\mathbf{r})$, corrected by the effective-mass terms following the procedure described in Refs. [29,31,56] are

$$V_N = V_N^{\text{SHF}} + \frac{\partial \varepsilon_{N\Lambda}}{\partial \rho_N} + \frac{\partial}{\partial \rho_N} \left(\frac{m_\Lambda}{m_\Lambda^*(\rho_N)} \right) \times \left(\frac{\tau_\Lambda}{2m_\Lambda} - \frac{3}{5} \frac{\rho_\Lambda (3\pi^2 \rho_\Lambda)^{2/3}}{2m_\Lambda} \right), \quad (4)$$

$$V_\Lambda = \frac{\partial(\varepsilon_{N\Lambda} + \varepsilon_{\Lambda\Lambda})}{\partial \rho_\Lambda} - \left(\frac{m_\Lambda}{m_\Lambda^*(\rho_N)} - 1 \right) \frac{(3\pi^2 \rho_\Lambda)^{2/3}}{2m_\Lambda}. \quad (5)$$

For the nucleonic part ε_{NN} , we use the Skyrme force SLy5 [55,61], which has been fit in a wide nuclear region. The energy density contributions $\varepsilon_{N\Lambda}$ [30,31] and $\varepsilon_{\Lambda\Lambda}$ [56] are parametrized as (ρ given in units of fm^{-3} , ε in MeV fm^{-3})

$$\varepsilon_{N\Lambda}(\rho_N, \rho_\Lambda) = -(\varepsilon_1 - \varepsilon_2 \rho_N + \varepsilon_3 \rho_N^2) \rho_N \rho_\Lambda + (\varepsilon_4 - \varepsilon_5 \rho_N + \varepsilon_6 \rho_N^2) \rho_N \rho_\Lambda^{5/3}, \quad (6)$$

$$\varepsilon_{\Lambda\Lambda}(\rho_\Lambda) = -\varepsilon_7 \rho_\Lambda^2 \Theta(N_\Lambda > 1), \quad (7)$$

together with

$$\frac{m_\Lambda^*}{m_\Lambda}(\rho_N) \approx \mu_1 - \mu_2 \rho_N + \mu_3 \rho_N^2 - \mu_4 \rho_N^3. \quad (8)$$

The parameters $\varepsilon_1, \dots, \varepsilon_6$ in Eq. (6) and the Λ effective-mass parameters μ_i in Eq. (8) were determined in BHF calculations of hypernuclear bulk matter with the Nijmegen potentials NSC89, NSC97a, and NSC97f [30,31], while the empirical expression involving the parameter ε_7 in Eq. (7) (labeled EmpC) has been proposed by fitting the bond energy of ${}_{\Lambda\Lambda}^6\text{He}$ in Ref. [56]. All parameters are listed in Table I. This procedure gives a good description of the binding energies of single- and double- Λ hypernuclei [29–31,56].

The pairing interaction is taken as a δ pairing force [62]:

$$V_q(\mathbf{r}_1, \mathbf{r}_2) = -V_0^{(q)} \delta(\mathbf{r}_1 - \mathbf{r}_2), \quad (9)$$

with the pairing strength $V_0^{(N)} = 323 \text{ MeV fm}^3$ for both neutrons and protons [62–64]. For Λ hyperons, as mentioned above, the pairing strength is set to 4/9 of this value [50], i.e., $V_0^{(\Lambda)} = 144 \text{ MeV fm}^3$. This pairing force is used within BCS approximation and a smooth energy cutoff is included [62]. In Ref. [50] a separable Gaussian pairing force was used instead, so that the absolute values of $V_0^{(\Lambda)}$ ($=324 \text{ MeV fm}^3$ in Ref. [50]) are not directly comparable. In the HFB calculations [28] the same nucleonic pairing strength as in our work was employed, but $V_0^{(\Lambda)}$ was calibrated to match the maximal value of the corresponding theoretical BCS prediction in uniform matter. This procedure yielded a pairing strength increasing with mass number, from 180 MeV fm^3 in Ca to 220 MeV fm^3 in Pb with the NSC97f model (together with a 60 MeV cutoff), cf. Table IV of Ref. [28]. These differences will become evident in the following discussion of the numerical results.

The pairing energies, to be added to the total energy (1), are given by

$$E_{\text{pair}}^q = \frac{1}{4} \int d^3r G_q(\mathbf{r}) \chi_q^*(\mathbf{r}) \chi_q(\mathbf{r}), \quad (10)$$

TABLE I. Parameters of the functionals Eqs. (6)–(8) of energy density and Λ effective mass [30,56] used in this work.

Functional	ε_1	ε_2	ε_3	ε_4	ε_5	ε_6	ε_7	μ_1	μ_2	μ_3	μ_4
NSC89 + EmpC	327	1159	1163	335	1102	1660	22.81	1.00	1.83	5.33	6.07
NSC97a + EmpC	423	1899	3795	577	4017	11061	21.12	0.98	1.72	3.18	0
NSC97f + EmpC	384	1473	1933	635	1829	4100	33.25	0.93	2.19	3.89	0

with the pairing strength $G_q(\mathbf{r}) = V_0^{(q)}$ under the assumption of the δ pairing force, and the pairing density matrix [62]

$$\chi_q(\mathbf{r}) = -2 \sum_{k \in \Omega_q, k > 0} u_q(k) v_q(k) |\phi_q^k(\mathbf{r})|^2, \quad (11)$$

with the pairing amplitudes $v_q(k)$ and $u_q(k) = [1 - v_q(k)^2]^{1/2}$. Here Ω_q is the set of projection of the total angular momentum of all s.p. states.

Furthermore, one can calculate the (average) pairing gap

$$\Delta_q \equiv \frac{\sum_{k \in \Omega_q} f_q(k) u_q(k) v_q(k) \Delta_q(k)}{\sum_{k \in \Omega_q} f_q(k) u_q(k) v_q(k)}, \quad (12)$$

where $\Delta_q(k) = \int d^3\mathbf{r} \phi_q^k(\mathbf{r})^\dagger \Delta_q(\mathbf{r}) \phi_q^k(\mathbf{r})$, $\Delta_q(\mathbf{r}) = \frac{1}{2} \chi_q(\mathbf{r}) G_q(\mathbf{r})$, and $f_q(k)$ are the state-dependent s.p. gap and smooth cutoff factor which can cure to some extent the defect of overestimating the coupling for the continuum states. Detailed discussions on this can be found in Ref. [62].

For the deformed nuclei in our approach, we assume axial symmetry of the mean field, and the deformed SHF Schrödinger equation is solved in cylindrical coordinates (r, z) within the axially deformed harmonic-oscillator basis [55,65]. The geometric quadrupole deformation parameter of the nuclear core is expressed as

$$\beta_2 \equiv \sqrt{\frac{\pi}{5}} \frac{\langle 2z^2 - r^2 \rangle}{\langle r^2 + z^2 \rangle}. \quad (13)$$

III. RESULTS

Since the $\Lambda\Lambda$ pairing force is the residual interaction of the two-body $\Lambda\Lambda$ interaction, before discussing the $\Lambda\Lambda$ pairing effects in hypernuclei, we first examine the EmpC prescription for the mean-field of the $\Lambda\Lambda$ interaction channel. For this purpose, we show in Fig. 1 the $\Lambda\Lambda$ separation energies $S_{\Lambda\Lambda} = E[{}^A Z] - E[{}^{A+2} Z]$ of the double- Λ hypernuclei ${}_{\Lambda\Lambda}^6\text{He}$, ${}_{\Lambda\Lambda}^{10,11,12}\text{Be}$, and ${}_{\Lambda\Lambda}^{12,13}\text{B}$, calculated by SHF using the NSC89,

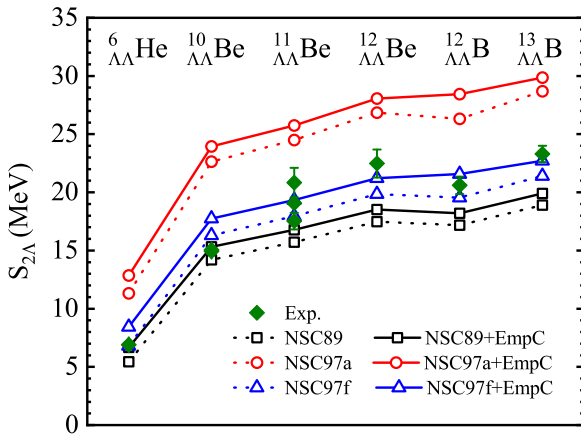


FIG. 1. The $\Lambda\Lambda$ separation energies of several double- Λ hypernuclei, calculated by SHF using the NSC89, NSC97a, and NSC97f ΛN interactions with and without EmpC prescription for the $\Lambda\Lambda$ channel, respectively. The experimental data are taken from Refs. [4,66]. Note that some data represent alternative interpretations of the same events, see the discussion in the text.

NSC97a, and NSC97f ΛN interactions with and without the EmpC prescription, in comparison with the corresponding experimental data tabulated in Refs. [4,43,66], derived from the KEK-E176 [67], KEK-E373 [68], and J-PARC-E07 [66] experiments.

The experimental data are obtained from candidate $\Lambda\Lambda$ -hypernuclear emulsion events. Reference [4] compares the experimental $\Lambda\Lambda$ separation energies with theoretical calculations using shell model and few-body cluster models, and the conclusions are as follows: So far, the only uniquely identified double- Λ hypernucleus is ${}_{\Lambda\Lambda}^6\text{He}$ (E373-NAGARA event) with $S_{2\Lambda} = 6.91 \pm 0.16$ MeV. Fitting this result, the binding energies of ${}_{\Lambda\Lambda}^{10}\text{Be}$ (E373-DEMACHIYANAGI, 14.94 ± 0.13 MeV) and ${}_{\Lambda\Lambda}^{13}\text{B}$ (E176-E4, 23.3 ± 0.7 MeV) were reproduced well by the shell model, which confirms the interpretations of the corresponding emulsion events. The E373-HIDA event does not allow any reasonable assignment as ${}_{\Lambda\Lambda}^{11,12}\text{Be}$ with 20.83 ± 1.27 or 22.48 ± 1.21 MeV, for which one of the alternative interpretations of E176 might be more suitable: ${}_{\Lambda\Lambda}^{11}\text{Be}$ (E176-G2, 17.53 ± 0.71 MeV) or ${}_{\Lambda\Lambda}^{12}\text{B}$ (E176-G3, 20.6 ± 0.74 MeV). Also, the ${}_{\Lambda\Lambda}^{10}\text{Be}$, 15.05 ± 0.11 MeV and the ${}_{\Lambda\Lambda}^{11}\text{Be}$, 19.07 ± 0.11 MeV interpretation of the most recently observed E07-MINO event [66] are compatible with this scenario. Altogether, the experimental situation is still hampered by the lack of uniquely identified events, which will hopefully improve in the near future.

In our theoretical model one observes that when including the EmpC prescription, the $B_{\Lambda\Lambda}$ values increase due to the attractive $\Lambda\Lambda$ interaction, which is fit to the NAGARA event. As a consequence, the NSC89 and NSC97f results become closer to the experimental data. Overall, the NSC97f + EmpC parameter set gives the best description for the experimental data. Therefore, we adopt this choice in the following.

Because current experimental data of multi- Λ hypernuclei only comprise double- Λ hypernuclei with hyperon shell closure, the $\Lambda\Lambda$ pairing effects vanish, and the $\Lambda\Lambda$ pairing strength cannot be determined from the double- Λ data.

Including the pairing force, Eq. (9), we will now first study the spherical multi- Λ hypernuclei with double closed nucleonic shells as in the HFB [28] and RHB [50] calculations, i.e., ${}_{-S\Lambda}^{40-S}\text{Ca}$, ${}_{-S\Lambda}^{132-S}\text{Sn}$, and ${}_{-S\Lambda}^{208-S}\text{Pb}$, and then study the deformed multi- Λ hypernuclei: ${}_{-S\Lambda}^{24-S}\text{Mg}$, ${}_{-S\Lambda}^{56-S}\text{Fe}$, and ${}_{-S\Lambda}^{104-S}\text{Zr}$.

A. Spherical hypernuclei

In Fig. 2, the $\Lambda\Lambda$ separation energies $S_{2\Lambda} \equiv E[{}_{(-S-2)\Lambda}^{A-S-2} Z] - E[{}_{-S\Lambda}^{A-S} Z]$, pairing gaps Δ_Λ , and pairing energies E_{pair}^Λ are displayed for the hyperisotopic chains ${}_{-S\Lambda}^{40-S}\text{Ca}$ ($-S = 0-20$), ${}_{-S\Lambda}^{132-S}\text{Sn}$ ($-S = 0-40$), and ${}_{-S\Lambda}^{208-S}\text{Pb}$ ($-S = 0-70$). The $\Lambda\Lambda$ separation energy indicates the location of Λ shell closures of hyperisotopes, where the pairing effects of hyperons vanish. The $\Lambda\Lambda$ pairing gap is one of the typical quantities to characterize pairing effects of hyperons. The pairing energy represents $\Lambda\Lambda$ pairing effects on the binding energy.

Before analyzing the results in detail, we comment that Λ -rich hypernuclei might be unstable due to the formation of $S = -2$ cascade hyperons by the $\Lambda\Lambda \rightarrow \Xi^- p$ reaction [56,69], which becomes energetically possible once $S_{2\Lambda} +$

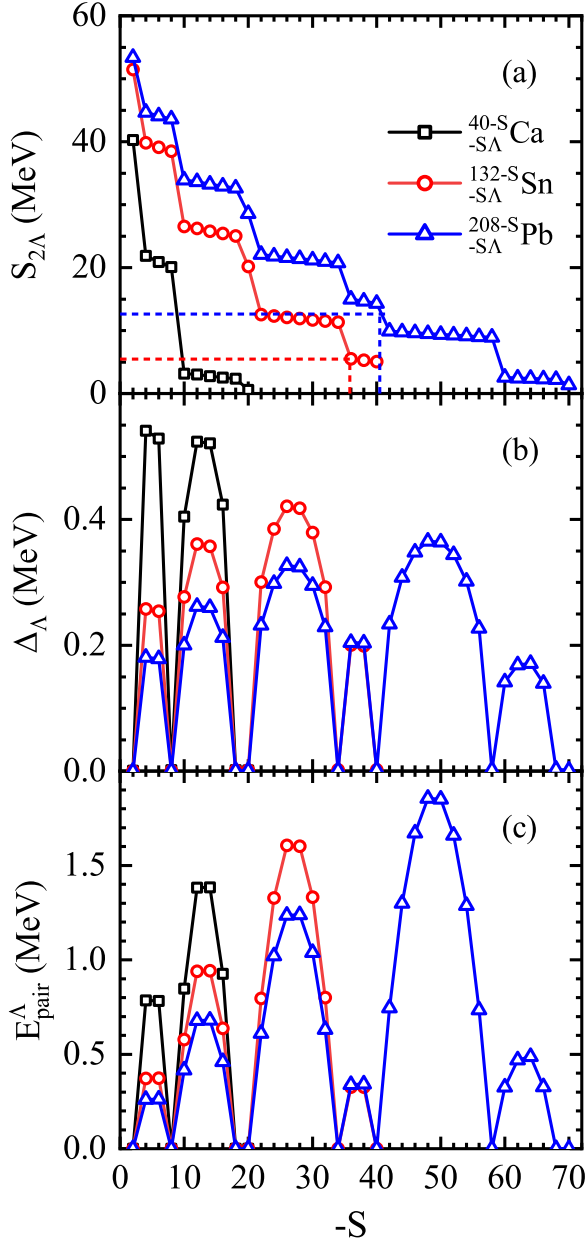


FIG. 2. (a) The $\Lambda\Lambda$ separation energies $S_{2\Lambda}$, (b) pairing gaps Δ_{Λ} , and (c) pairing energies $E_{\text{pair}}^{\Lambda}$ for Ca, Sn, and Pb hyperisotopic chains, obtained with the NSC97f + EmpC parameter set. Estimates of the instability due to Ξ^- formation are indicated by dashed lines.

$28.6 \text{ MeV} < S_{\Xi^-} + S_p$, where S_{Ξ^-} and S_p are the relevant single-baryon separation energies. Using a recent determination of the Ξ^-p interaction [70] (and ignoring the unknown $\Lambda\Xi$ interaction) this occurs at $-S \approx 36$ and 42 for Sn and Pb cores, respectively, which are indicated by dashed lines in the figure. In this sense the following results obtained for larger $-S$ values are purely theoretical. The alternative $\Lambda\Lambda \rightarrow \Xi^0 n$ reaction is not accessible due to the more attractive Coulomb-assisted Ξ^-p mode in nearly symmetric finite nuclei.

As indicated in Fig. 2(a), $S_{2\Lambda}$ features sudden drops at $-S = 2, 8, 18, 20, 34, 40, 58, 68$, and 70 , which indicate the magic numbers of hyperisotopes (corresponding to shell

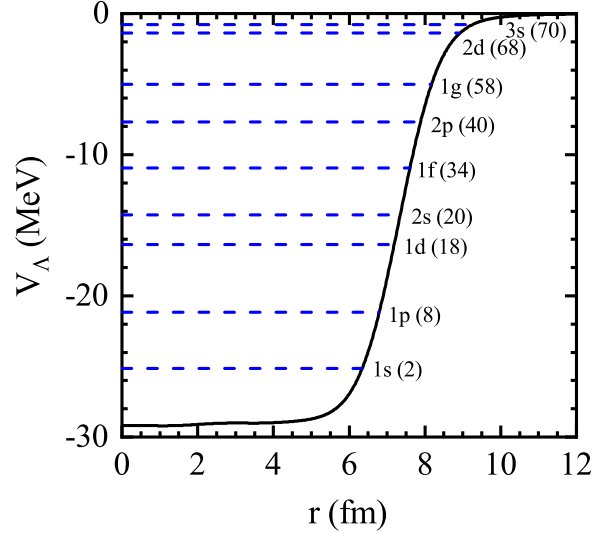


FIG. 3. The Λ hyperon potential V_{Λ} and s.p. levels for $^{278}_{70\Lambda}\text{Pb}$ in the SHF approach with the parameter set NSC97f + EmpC.

closures), where the $\Lambda\Lambda$ pairing gap Δ_{Λ} , plotted in Fig. 2(b), vanishes. Due to the absence of relevant Λ spin-orbit forces, the individual shells are fairly large and therefore allow strong pairing correlations for hyperisotopes located close to their center: The gap reaches about 0.55 , 0.40 , and 0.35 MeV in half-filled shell hypernuclei for Ca, Sn, and Pb isotopes, respectively. The same shell structure is also found for the pairing energies $E_{\text{pair}}^{\Lambda}$ shown in Fig. 2(c), namely, zero values at closed shells and maximal values for half-filled shell.

Compared with the RHB calculations with the effective interactions PK1-Y1 and NLSH-A [50], one notes that the Λ subshell closures are not exactly the same as in SHF. For example, Δ_{Λ} does not vanish for $^{58}_{18\Lambda}\text{Ca}$ (both parameter sets) and for $^{276}_{68\Lambda}\text{Pb}$ (PK1-Y1 parameters). Also, slightly larger maximal pairing gaps (about 0.8 , 0.6 , and 0.5 MeV for Ca, Sn, Pb) were obtained in the RHB model, which are due to the stronger $\Lambda\Lambda$ pairing force.

In the previous HFB work [28], Λ gaps were not reported, while the pairing energies were defined as the energy difference between HF and HFB calculations, $E_{\text{HF}} - E_{\text{HFB}}$, and a maximum value of ≈ 3 MeV was obtained for Sn isotopes, which is larger than ours due to a much larger pairing strength used there, see the discussion in Sec. II above.

The reason for the additional Λ shell closures at $-S = 18$ and 68 in SHF is explored in Fig. 3, where we plot the Λ mean field V_{Λ} and the s.p. levels for $^{278}_{70\Lambda}\text{Pb}$ as an example. Because of a lacking spin-orbit term, the magic numbers of hyperons are not the same as for nucleons ($2, 8, 20, 28, 50, 82, \dots$). V_{Λ} is a Woods-Saxon-like potential, which results in the corresponding shell structure [71], as also in Ref. [28] due to the same mean-field potential of hyperons. On the contrary, V_{Λ} obtained in the RHB calculation [50] is similar to a harmonic-oscillator potential and leads to slightly different shell closures. One observes in any case that the SHF shells at $-S = 18$ and 20 and at 68 and 70 are nearly degenerate in energy.

Figure 4 compares the Λ gaps obtained in the SHF, HFB [28], and RHB [50] approaches for the nuclei $^{46}_{6\Lambda}\text{Ca}$, $^{160}_{28\Lambda}\text{Sn}$,

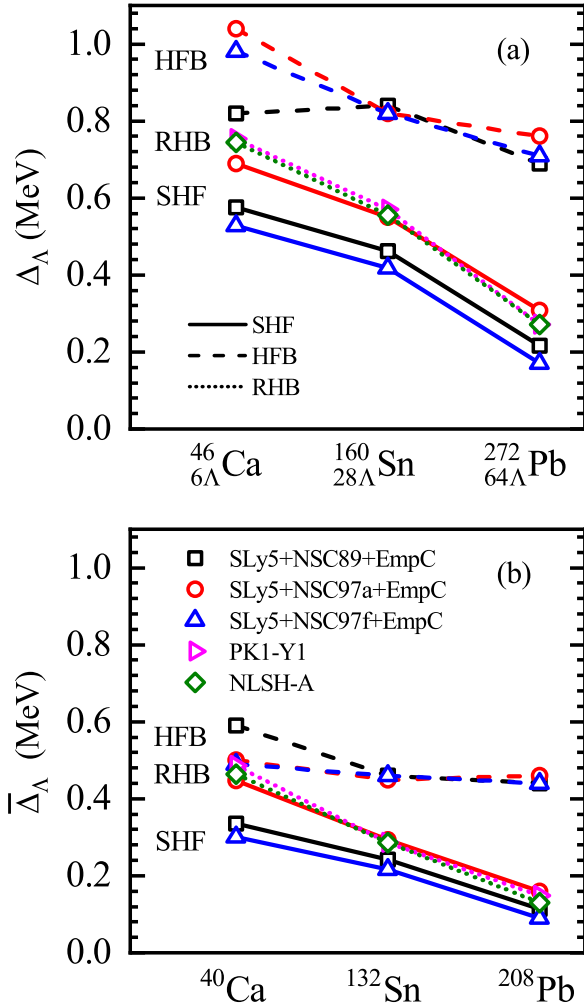


FIG. 4. (a) The pairing gaps Δ_Λ for $^{46}_{6\Lambda}\text{Ca}$, $^{160}_{28\Lambda}\text{Sn}$, and $^{272}_{64\Lambda}\text{Pb}$. (b) The average gaps $\bar{\Delta}_\Lambda$, Eq. (14), for ^{40}Ca ($-S = 6-20$), ^{132}Sn ($-S = 18-40$), and ^{208}Pb ($-S = 58-70$) hyperisotopes in the SHF and HFB [28] approaches using the NSC89/97a/97f + EmpC parameter sets, and in the RHB approach with the PK1-Y1 and NLSH-A forces [50].

and $^{272}_{64\Lambda}\text{Pb}$, and also the gap averaged over a range of the hyperisotopic chain,

$$\bar{\Delta}_\Lambda(^AZ) \equiv \langle \Delta_\Lambda(^{A-S}_{-S\Lambda}Z) \rangle_S, \quad (14)$$

for $Z = \text{Ca}$ ($-S = 6-20$), Sn ($-S = 18-40$), and Pb ($-S = 58-70$), as in Ref. [50]. The gaps in HFB are larger than those in SHF and RHB due to the larger pairing strength employed, and the slower decreasing trend with mass number in the HFB calculation is caused by the gradually increased pairing strength (cf. Table IV of Ref. [28]). With the same treatment of the $\Lambda\Lambda$ pairing strength, the SHF and RHB results are very similar, in particular for the SHF NSC97a model. The differences between the NSC89/97a/97f models in SHF and RHB are caused by different Λ s.p. properties, see also Fig. 1.

B. Deformed hypernuclei

We now extend the study of the $\Lambda\Lambda$ pairing effects to the typical deformed-core nuclei ^{24}Mg , ^{56}Fe , and ^{104}Zr for

the first time. In general, deformation causes the splitting of the spherical orbits into smaller subshells and consequently reduces the possibility and strength of the pairing phenomenon [72]. This can be seen in the following results.

In Fig. 5, the deformations β_2 , 2Λ separation energies $S_{2\Lambda}$, pairing gaps Δ_Λ , and pairing energies E_{pair}^Λ are shown for the hyperisotopes $^{24-S}_{-S\Lambda}\text{Mg}$ ($-S = 0-8$), $^{56-S}_{-S\Lambda}\text{Fe}$ ($-S = 0-18$), and $^{104-S}_{-S\Lambda}\text{Zr}$ ($-S = 0-34$) with NSC97f + EmpC parameter set. According to Fig. 5(b), at least 8, 18, and 34 hyperons can be bound to the core nuclei ^{24}Mg , ^{56}Fe , and ^{104}Zr , respectively. However, Ξ^- formation imposes a limit $-S < 28$ for Zr. As indicated in Fig. 5(a), not only the normal nuclei ($-S = 0$), but also the hypernuclei for all isotopes are well-deformed, mostly prolate, but some Zr hyperisotopes are oblate. Due to the splitting of the s.p. states caused by the deformation, the $S_{2\Lambda}$ values drop more regularly than for spherical nuclei, and it is more difficult to identify obvious steps corresponding to shell closure, also because the physical deformation β_2 might change rapidly with $-S$.

However, all deformed hyperisotopes show vanished Δ_Λ and E_{pair}^Λ at $-S = 2, 4, 8, 10, 14, 18, 20, 22, 26, 30, 32$, and 34, and the Zr hyperisotopes in addition at $-S = 6$. This provides the evidence for the appearance of the new possible magic numbers $-S = 4, 6, 10, 14, 26, 30$, and 32 in the deformed hyperisotopes. In other words, pairing occurs only for partially filled shells at $-S = 6, 12, 16, 24$, and 28.

To further explore the above features, we show in Fig. 6(a) the hyperon s.p. energies as functions of deformation β_2 for $^{130}_{26\Lambda}\text{Zr}$. Due to the absence of a spin-orbit potential, the spin-orbit partner levels are degenerate at spherical shape $\beta_2 = 0$. One observes that there are large gaps at $-S = 2, 4, 8, 10, 14, 18, 20, 22, 26, 30, 32$, and 34 on the prolate side, which explains the behavior of $S_{2\Lambda}$, Δ_Λ , and E_{pair}^Λ shown in Fig. 5.

The sudden drop of $S_{2\Lambda}$ in $^{24-S}_{-S\Lambda}\text{Mg}$ at $-S = 4$ is attributed to the large gap between the [110] and [101] orbits at $\beta_2 \approx 0.4$ (the actual deformation of $^{28}_{4\Lambda}\text{Mg}$ and $^{30}_{6\Lambda}\text{Mg}$). For prolate and oblate hypernuclei, the [101 1/2] and [101 3/2] orbits are degenerate, which explains why the pairing of hyperons vanishes for the oblate $^{110}_{6\Lambda}\text{Zr}$, but not for the prolate $^{30}_{6\Lambda}\text{Mg}$ and $^{62}_{6\Lambda}\text{Fe}$. From the figure it is also clear that the possible magic numbers (shell closures) in deformed hypernuclei are sensitive to β_2 due to the possible crossing of some s.p. levels.

The reason for the suppression of pairing in deformed isotopes that exhibit strong gaps in a spherical calculation is that the previously partially occupied shells are now splitting into well separated full and empty shells. This is illustrated in Figs. 6(b) and 6(c), which show the pairing gap and the occupation probability of the $1f$ sublevels of $^{130}_{26\Lambda}\text{Zr}$ as a function of deformation β_2 . One can clearly see that the gap drops fast from its undeformed value ≈ 0.4 MeV, see also Fig. 2, to vanish at $\beta_2 \approx 0.2$, and remains zero at the actual deformation $\beta_2 \approx 0.4$. This is caused by the splitting of the undeformed $1f$ level into a completely occupied [310 + 321] level that becomes well separated from the neighboring empty [301 + 312] level. Once the separation of these levels becomes much larger than the (spherical) pairing gap, the gap vanishes. The result is even more interesting for oblate deformation, where $\Delta_\Lambda(\beta_2)$ exhibits nonmonotonic behavior due to the crossing

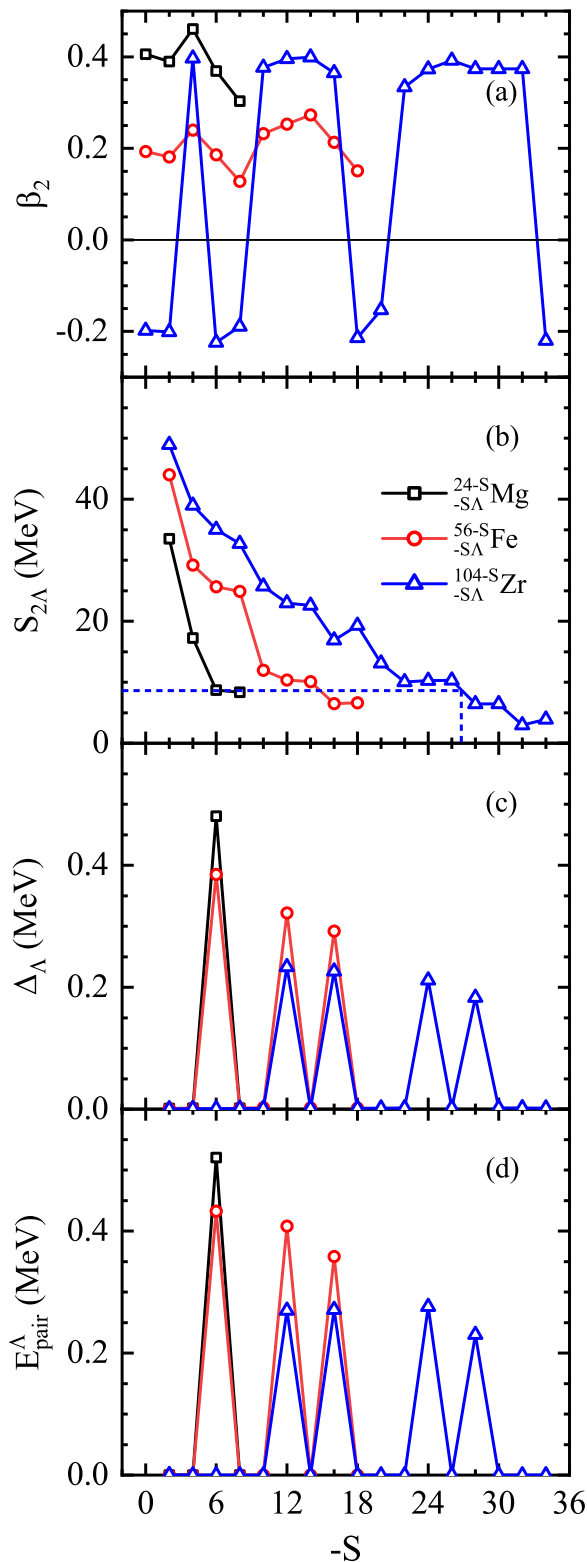


FIG. 5. (a) The quadrupole deformations β_2 , (b) the 2Λ separation energies $S_{2\Lambda}$, (c) the pairing gaps Δ_Λ , and (d) the pairing energies E_{pair}^Λ for Mg, Fe, and Zr hyperisotopes obtained with NSC97f + EmpC parameter set. Estimates of the instability due to e^- formation are indicated by dashed lines.

of the $[310 + 321]$ and $[301 + 312]$ levels, and vanishes only at $\beta_2 \approx -0.4$. The dependence of the pairing gap on β_2 is also illustrated by the corresponding occupations of the various involved $1f$ sublevels shown in Fig. 6(c).

In other words, the pairing effect depends on the s.p. level density around the Fermi surface. The pairing gap for prolate deformation vanishes gradually because the levels become more separated at larger deformation, whereas the interesting behavior of the pairing gap for oblate deformation can be explained by the irregular distribution of the s.p. energy levels and their crossings. In general, however, deformation always leads to a weakening or complete suppression of pairing.

IV. CONCLUSIONS

We explored the $\Lambda\Lambda$ pairing effects in spherical $^{40-S}_{-S\Lambda}\text{Ca}$, $^{132-S}_{-S\Lambda}\text{Sn}$, $^{208-S}_{-S\Lambda}\text{Pb}$, and deformed $^{24-S}_{-S\Lambda}\text{Mg}$, $^{56-S}_{-S\Lambda}\text{Fe}$, $^{104-S}_{-S\Lambda}\text{Zr}$ multi- Λ hypernuclei in the framework of the SHF approach with the Skyrme force SLy5 for the NN interaction, the Nijmegen interaction NSC97f for the ΛN interaction, and the empirical prescription EmpC for the $\Lambda\Lambda$ interaction. The $\Lambda\Lambda$ pairing interaction is modeled by a δ force with a pairing strength assumed as $4/9$ of that for nucleons.

For the spherical hyperisotopes, the occurrences of magic numbers $-S = 2, 8, 18, 20, 34, 58, 68,$ and 70 are evinced by the sudden drop of 2Λ separation energies and the vanished average pairing gaps and pairing energies due to a Woods-Saxon-like Λ hyperon potential. For the deformed hyperisotopes, more possible hyperon magic numbers $-S = 4, 6, 10, 14, 22, 26, 30,$ and 32 corresponding to vanishing pairing appear. They are different from the conventional nucleon magic numbers due to the negligible spin-orbit interaction. All possible hyperon magic numbers of the deformed hyperisotopes are sensitive to β_2 based on the analysis of the s.p. energy levels. Because deformation causes a splitting into smaller subshells with smaller mutual separation, the 2Λ separation energy drops at shell closure such as at $-S = 4, 6, 10, 14,$ and 32 are smaller than those occurring in spherical systems and no longer a good indicator for magicity. This is accompanied by a strong reduction or complete disappearance of pairing for well-deformed hypernuclei.

In addition, the current work predicts similar pairing gap results as a RHB approach, but smaller ones than those in a HFB approach due to a smaller pairing strength. In all cases, the hyperon gaps are much smaller than the nucleonic ones, and in deformed nuclei the pairing correlations are even weaker.

However, we stress that the $\Lambda\Lambda$ pairing strengths in all current works are based on purely theoretical conjectures and require confrontation with experimental data for quantitative confirmation and improvement. It is currently not even certain that $\Lambda\Lambda$ pairing exists. Multi- Λ hypernuclei should be studied in future experiments to improve our understanding of the $\Lambda\Lambda$ interaction channel.

ACKNOWLEDGMENT

This work was supported by the National Natural Science Foundation of China under Grants No. 12175071 and No. 11775081.

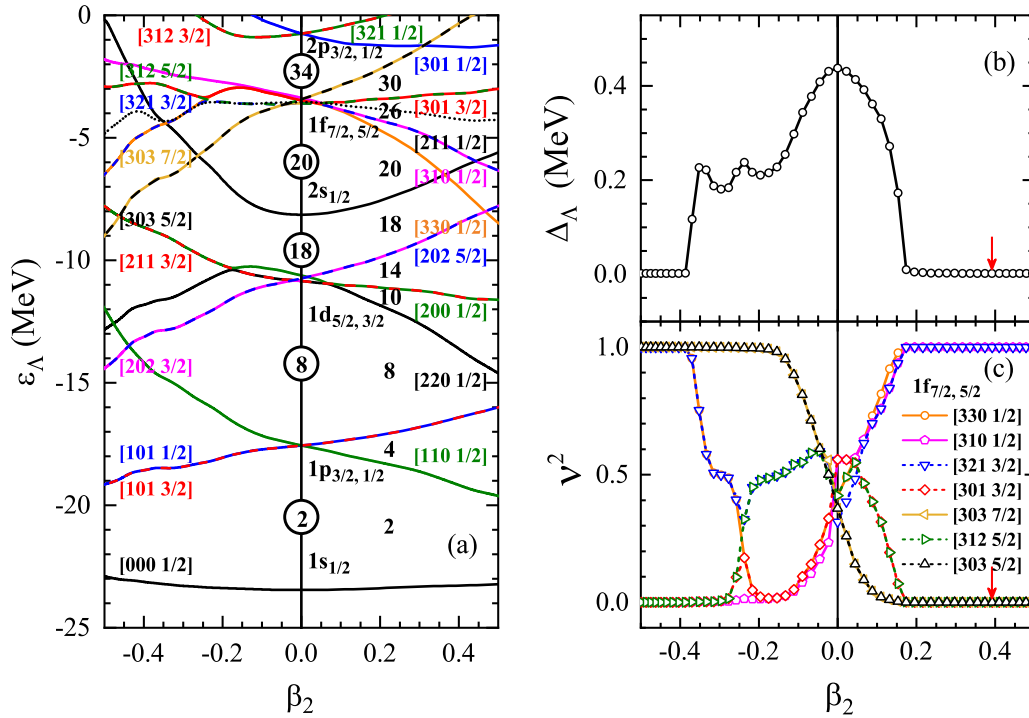


FIG. 6. Several quantities of the hypernucleus $^{130}_{26}\Lambda\text{Zr}$ with NSC97f + EmpC parameter set as a function of deformation β_2 : (a) The Λ s.p. energies. The Fermi surface is indicated by the dotted black curve. The quantum numbers for the spherical orbits are labeled around $\beta_2 = 0$, and the deformed quantum numbers $[Nn_z m_l \Omega]$ along the curves. Also indicated are the magic numbers in the spherical and prolate cases. (b) The Λ pairing gap. (c) The Λ occupation probability v^2 of the $1f$ sublevels. The actual deformation $\beta_2 \approx 0.40$ of this hypernucleus is also indicated.

[1] M. Danysz and J. Pniewski, *Philos. Mag.* **44**, 348 (1953).
 [2] O. Hashimoto and H. Tamura, *Prog. Part. Nucl. Phys.* **57**, 564 (2006).
 [3] A. Feliciello and T. Nagae, *Rep. Prog. Phys.* **78**, 096301 (2015).
 [4] A. Gal, E. V. Hungerford, and D. J. Millener, *Rev. Mod. Phys.* **88**, 035004 (2016).
 [5] E. Hiyama and K. Nakazawa, *Annu. Rev. Nucl. Part. Sci.* **68**, 131 (2018).
 [6] M. Rayet, *Nucl. Phys. A* **367**, 381 (1981).
 [7] D. J. Millener, C. B. Dover, and A. Gal, *Phys. Rev. C* **38**, 2700 (1988).
 [8] X.-R. Zhou, H.-J. Schulze, H. Sagawa, C.-X. Wu, and E.-G. Zhao, *Phys. Rev. C* **76**, 034312 (2007).
 [9] X.-R. Zhou, A. Polls, H.-J. Schulze, and I. Vidaña, *Phys. Rev. C* **78**, 054306 (2008).
 [10] X. R. Zhou, J. W. Cui, and N. Wei, *Sci. China, Ser. G: Phys., Mech. Astron.* **52**, 1548 (2009).
 [11] H.-J. Schulze, M. Thi Win, K. Hagino, and H. Sagawa, *Prog. Theor. Phys.* **123**, 569 (2010).
 [12] M. T. Win, K. Hagino, and T. Koike, *Phys. Rev. C* **83**, 014301 (2011).
 [13] H.-J. Schulze and E. Hiyama, *Phys. Rev. C* **90**, 047301 (2014).
 [14] B.-C. Fang, W.-Y. Li, C.-F. Chen, J.-W. Cui, X.-R. Zhou, and Y.-Y. Cheng, *Eur. Phys. J. A* **56**, 11 (2020).
 [15] Y. Zhang, H. Sagawa, and E. Hiyama, *Phys. Rev. C* **103**, 034321 (2021).
 [16] Y.-S. Shen and Z.-Z. Ren, *Acta Phys. Sin. (Overseas Ed.)* **7**, 258 (1998).
 [17] H. F. Lü, J. Meng, S. Q. Zhang, and S.-G. Zhou, *Eur. Phys. J. A* **17**, 19 (2003).
 [18] H. Shen, F. Yang, and H. Toki, *Prog. Theor. Phys.* **115**, 325 (2006).
 [19] B.-N. Lu, E.-G. Zhao, and S.-G. Zhou, *Phys. Rev. C* **84**, 014328 (2011).
 [20] C. Y. Song, J. M. Yao, and J. Meng, *Chin. Phys. Lett.* **28**, 092101 (2011).
 [21] R. L. Xu, C. Wu, and Z. Z. Ren, *J. Phys. G* **39**, 085107 (2012).
 [22] B. Bhowmick, A. Bhattacharyya, and G. Gangopadhyay, *Eur. Phys. J. A* **50**, 125 (2014).
 [23] B.-N. Lu, E. Hiyama, H. Sagawa, and S.-G. Zhou, *Phys. Rev. C* **89**, 044307 (2014).
 [24] S.-H. Ren, T.-T. Sun, and W. Zhang, *Phys. Rev. C* **95**, 054318 (2017).
 [25] T.-T. Sun, W.-L. Lu, and S.-S. Zhang, *Phys. Rev. C* **96**, 044312 (2017).
 [26] Z.-X. Liu, C.-J. Xia, W.-L. Lu, Y.-X. Li, J. N. Hu, and T.-T. Sun, *Phys. Rev. C* **98**, 024316 (2018).
 [27] Y. Tanimura, *Phys. Rev. C* **99**, 034324 (2019).
 [28] H. Güven, K. Bozkurt, E. Khan, and J. Margueron, *Phys. Rev. C* **98**, 014318 (2018).
 [29] J. Cugnon, A. Lejeune, and H.-J. Schulze, *Phys. Rev. C* **62**, 064308 (2000).

- [30] I. Vidaña, A. Polls, A. Ramos, and H.-J. Schulze, *Phys. Rev. C* **64**, 044301 (2001).
- [31] H.-J. Schulze and T. Rijken, *Phys. Rev. C* **88**, 024322 (2013).
- [32] E. Khan, J. Margueron, F. Gulminelli, and A. R. Raduta, *Phys. Rev. C* **92**, 044313 (2015).
- [33] H. Mei, K. Hagino, J. M. Yao, and T. Motoba, *Phys. Rev. C* **91**, 064305 (2015).
- [34] J.-W. Cui, X.-R. Zhou, L.-X. Guo, and H.-J. Schulze, *Phys. Rev. C* **95**, 024323 (2017).
- [35] J.-W. Cui and X.-R. Zhou, *Prog. Theor. Exp. Phys.* **2017**, 093D04 (2017).
- [36] X. Y. Wu, H. Mei, J. M. Yao, and X.-R. Zhou, *Phys. Rev. C* **95**, 034309 (2017).
- [37] W.-Y. Li, J.-W. Cui, and X.-R. Zhou, *Phys. Rev. C* **97**, 034302 (2018).
- [38] H. Mei, K. Hagino, J. M. Yao, and T. Motoba, *Phys. Rev. C* **97**, 064318 (2018).
- [39] H. Xia, X. Wu, H. Mei, and J. Yao, *Sci. China: Phys., Mech. Astron.* **62**, 42011 (2019).
- [40] E. Hiyama, M. Kamimura, T. Motoba, T. Yamada, and Y. Yamamoto, *Phys. Rev. C* **66**, 024007 (2002).
- [41] E. Hiyama and T. Yamada, *Prog. Part. Nucl. Phys.* **63**, 339 (2009).
- [42] H. Le, J. Haidenbauer, U.-G. Meißner, and A. Nogga, *Eur. Phys. J. A* **56**, 301 (2020).
- [43] A. Gal and D. J. Millener, *Phys. Lett. B* **701**, 342 (2011).
- [44] S. Balberg and N. Barnea, *Phys. Rev. C* **57**, 409 (1998).
- [45] T. Takatsuka and R. Tamagaki, *Nucl. Phys. A* **670**, 222 (2000).
- [46] T. Takatsuka, S. Nishizaki, Y. Yamamoto, and R. Tamagaki, *Nucl. Phys. A* **691**, 254 (2001).
- [47] T. Tanigawa, M. Matsuzaki, and S. Chiba, *Phys. Rev. C* **68**, 015801 (2003).
- [48] Y. N. Wang and H. Shen, *Phys. Rev. C* **81**, 025801 (2010).
- [49] A. R. Raduta, A. Sedrakian, and F. Weber, *Mon. Not. R. Astron. Soc.* **475**, 4347 (2018).
- [50] Y.-T. Rong, P. Zhao, and S.-G. Zhou, *Phys. Lett. B* **807**, 135533 (2020).
- [51] S. Schramm, *Phys. Rev. C* **66**, 064310 (2002).
- [52] A. Bhagwat, X. Viñas, M. Centelles, P. Schuck, and R. Wyss, *Phys. Rev. C* **86**, 044316 (2012).
- [53] R. Xu, C. Wu, G. Ma, D. Fang, and Z. Ren, *Phys. Rev. C* **87**, 014335 (2013).
- [54] T. Togashi, Y. Tsunoda, T. Otsuka, and N. Shimizu, *Phys. Rev. Lett.* **117**, 172502 (2016).
- [55] M. Bender, P. H. Heenen, and P. G. Reinhard, *Rev. Mod. Phys.* **75**, 121 (2003).
- [56] J. Margueron, E. Khan, and F. Gulminelli, *Phys. Rev. C* **96**, 054317 (2017).
- [57] D. Vautherin and D. M. Brink, *Phys. Rev. C* **5**, 626 (1972).
- [58] M. Bender, K. Rutz, P.-G. Reinhard, J. A. Maruhn, and W. Greiner, *Phys. Rev. C* **60**, 034304 (1999).
- [59] W. Brückner *et al.*, *Phys. Lett. B* **79**, 157 (1978).
- [60] S. Ajimura, H. Hayakawa, T. Kishimoto, H. Kohri, K. Matsuoka, S. Minami, T. Mori, K. Morikubo, E. Saji, A. Sakaguchi, Y. Shimizu, M. Sumihama, R. E. Chrien, M. May, P. Pile, A. Rusek, R. Sutter, P. Eugenio, G. Franklin, P. Khaustov, K. Paschke, B. P. Quinn, R. A. Schumacher, J. Franz, T. Fukuda, H. Noumi, H. Outa, L. Gan, L. Tang, L. Yuan, H. Tamura, J. Nakano, T. Tamagawa, K. Tanida, and R. Sawafuta, *Phys. Rev. Lett.* **86**, 4255 (2001).
- [61] E. Chabanat, P. Bonche, P. Haensel, J. Meyer, and R. Schaeffer, *Nucl. Phys. A* **635**, 231 (1998).
- [62] M. Bender, K. Rutz, P. G. Reinhard, and J. A. Maruhn, *Eur. Phys. J. A* **8**, 59 (2000).
- [63] S. Yoshida and H. Sagawa, *Phys. Rev. C* **77**, 054308 (2008).
- [64] Z.-J. Luo, K. Yu, X.-R. Zhou, J.-W. Cui, and H. Sagawa, *Eur. Phys. J. A* **54**, 1 (2018).
- [65] D. Vautherin, *Phys. Rev. C* **7**, 296 (1973).
- [66] H. Ekawa *et al.*, *Prog. Theor. Exp. Phys.* **2019**, 021D02 (2019).
- [67] S. Aoki *et al.* (KEK E176 Collaboration), *Nucl. Phys. A* **828**, 191 (2009).
- [68] J. K. Ahn *et al.* (KEK-PS E373 Collaboration), *Phys. Rev. C* **88**, 014003 (2013).
- [69] J. Schaffner, C. B. Dover, A. Gal, C. Greiner, D. J. Millener, and H. Stöcker, *Ann. Phys. (NY)* **235**, 35 (1994).
- [70] J. Guo, X.-R. Zhou, and H.-J. Schulze, *Phys. Rev. C* **104**, L061307 (2021).
- [71] P. Ring and P. Schuck, *The Nuclear Many-Body Problem* (Springer Science & Business Media, Berlin, 1980).
- [72] L. M. Robledo, R. Bernard, and G. F. Bertsch, *Phys. Rev. C* **86**, 064313 (2012).